nature structural & molecular biology

Allosteric enhancement of MAP kinase p38α's activity and substrate selectivity by docking interactions

Yuji Tokunaga[1,2], Koh Takeuchi[3], Hideo Takahashi[3,4] & Ichio Shimada[2,3]

Mitogen-activated protein kinases (MAPKs) are essential to intracellular signal transduction. MAPKs anchor their pathway-specific substrates through so-called 'docking interactions' at locations distal from the active site. Docking interactions ensure efficient substrate recognition, but their contribution to the kinase reaction itself remains unclear. Herein, we use solution NMR to analyze the interaction between dually phosphorylated, active human p38α and the C-terminal fragments of its substrate MK2. p38α phosphorylation and ATP loading collaboratively induce the active conformation; subsequently, p38α accommodates MK2 phosphoacceptor residues in its active site. The docking interaction enhances binding of ATP and the phosphoacceptor to p38α, accelerating the phosphotransfer reaction. Thus, the docking interaction enhances p38α's enzymatic activity toward pathway-specific substrates allosterically as well as by the anchor effect. These findings clarify how MAPK cascades are organized in cells, even under ATP-depleted conditions often associated with environmental stress.

© 2014 Nature America, Inc. All rights reserved.

MAPKs have pivotal roles in intracellular signal transduction, the process of converting various stimuli into corresponding cellular events[1–5]. An isoform of the p38 subfamily, p38α, mediates stress-induced apoptosis[6] and is involved in the production of inflammatory cytokines, including tumor necrosis factor α, thus making the protein a potential drug target for inflammatory diseases[7,8]. Because of the importance of MAPKs in various cellular functions, MAPK signals must be strictly regulated to elicit the correct cellular responses[1,5]. MAPKs are controlled in a common scheme called the MAPK cascade, which is characterized by the stepwise phosphorylation of three tiers of hierarchical kinases: MAPK kinase kinase, MAPK kinase (MAPKK) and MAPK[9]. The activated MAPKK dually phosphorylates MAPK at the threonine and tyrosine residues in the conserved TXY motif, which is required for the full activation of MAPK[10,11]. The activated MAPK phosphorylates its substrates to evoke cellular responses[3] that are subsequently turned off by their specific phosphatases[12].

MAPKs consist of a typical kinase domain composed of N and C lobes[13–15]. The N lobe binds ATP, and the C lobe contains the P+1 site, to which the substrate's phosphoacceptor residues localize during the phosphotransfer reaction (**Fig. 1a**). An activation loop, which contains the TXY phosphorylation motif (180-TGY-182 for p38α), lies in a groove between these two lobes. Whereas the N and C lobes are spatially separated to form an 'open' conformation in unphosphorylated, inactive MAPKs (for example, PDB 1P38 (ref. 14) and 1WFC[15] for p38α and 1ERK[16] for ERK2), the distance between these two lobes decreases to form a 'closed' conformation in the crystal structure of phosphorylated p38γ bound to adenylyl imidodiphosphate (AMP-PNP; PDB 1CM8 (ref. 17)). Such closure is essential for efficient phosphotransfer because the spatial proximity of the γ-phosphate of ATP, which binds the N lobe, and the hydroxyl groups of the substrate phosphoacceptor residues trapped in the C lobe are a prerequisite for the reaction[17,18]. Crystal structures of phosphorylated apo-MAPKs have been solved in both closed (ERK2, PDB 2ERK[18]) and open (p38α, PDB 3PY3 (ref. 19)) conformations. This suggests that the dual phosphorylation itself may not always coincide with formation of the closed, active conformation of MAPK.

The specific interactions of MAPKs with MAPKKs, substrates and phosphatases rely on conserved docking interactions[20–26] that use sites distal from the active sites in MAPKs and functional sites in the binding partners (for example, the substrate phosphoacceptor sites). In the case of a p38α substrate, MAP kinase–activated protein kinase 2 (MK2), a C-terminal, 30-residue sequence (amino acids (aa) 371–400) is responsible for binding to p38α, while the phosphoacceptor residues, Thr222, Ser272 and Thr334, are distant from the docking sequence (**Fig. 1b**). Deletion of the C-terminal docking sequence in MK2 impairs binding and efficient phosphorylation by p38α (ref. 27). The p38α crystal structures solved in complex with various docking sequences indicate that p38α accommodates the docking sequences in a site located opposite to its active site[28,29] (**Fig. 1a**), and differences in the amino acid compositions of the docking sequences determine the specificity toward the partner molecules[22,30,31]. Therefore, the docking interaction is the key mechanism through which the MAPKs efficiently discriminate their binding partners from the other proteins within the same signaling pathway.

The consensus motif of the MAPK substrate phosphoacceptor site contains serine or threonine followed by proline at the +1 position and a preference for proline at −2. This simple motif overlaps with the phosphorylation motifs of other kinases[32] and thus is not sufficient to

[1]Research and Development Department, Japan Biological Informatics Consortium, Tokyo, Japan. [2]Graduate School of Pharmaceutical Sciences, University of Tokyo, Tokyo, Japan. [3]Biomedicinal Information Research Center, National Institute of Advanced Industrial Science and Technology, Tokyo, Japan. [4]Graduate School of Medical Life Science, Yokohama City University, Kanagawa, Japan. Correspondence should be addressed to I.S. (shimada@iw-nmr.f.u-tokyo.ac.jp).

Received 26 February; accepted 19 June; published online 20 July 2014; doi:10.1038/nsmb.2861

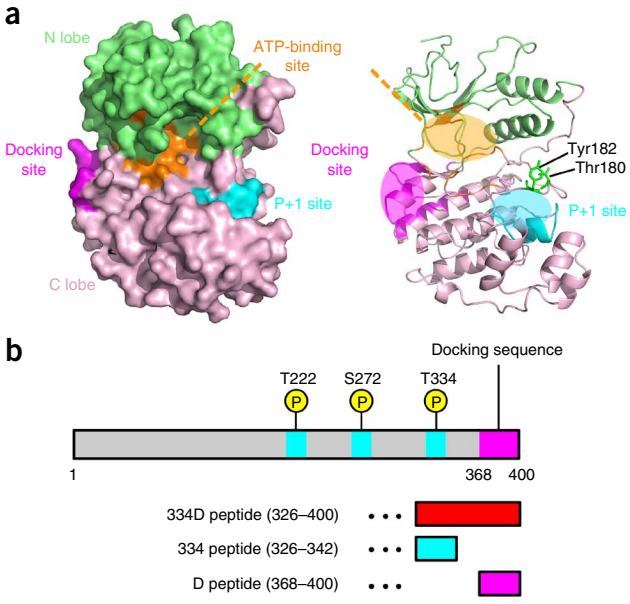

Figure 1 Functional sites in p38α and the substrate peptides used in this study. (**a**) Surface (left) and ribbon (right) representations of a model structure of the dually phosphorylated p38α. The model was generated by the SWISS-MODEL server[50], with the crystal structure of p38γ-2P in complex with AMP-PNP (PDB 1CM8 (ref. 17)) as the template. The structure of bound AMP-PNP was omitted in the figure. The N and C lobes are colored green and pink, respectively. At right, Thr180 and Tyr182 in the activation loop, which are phosphorylated by MAPKK, are indicated by green stick representations, and the ATP-binding site, the P+1 site and the docking site are indicated by orange, cyan and magenta circles, respectively. (**b**) Schematic representation of the p38α substrate, MK2 and the peptides derived from MK2 used in this study.

determine the target specificities of MAPKs. The structural mechanisms underlying phosphoacceptor binding and phosphotransfer are not well understood. The reported structures for a MAPK in complex with a phosphoacceptor-containing substrate are of unphosphorylated p38α (PDB 2ONL[29] and 2OZA[33]). However, these structures cannot explain the phosphotransfer mechanism because the phosphoacceptor residues of the substrate, MK2, do not bind to the P+1 site of p38α. The absence of the interaction may arise from the use of the unphosphorylated, inactive p38α for the structural analysis. In addition, it is not clear whether the docking interaction is used only to tether the substrate and increase the local concentration of phosphoacceptor sites or whether it has additional allosteric effects on the enzymatic activity of MAPK. A previous kinetic analysis showed that ATP and a substrate, activating transcription factor 2 (ATF2), cooperatively enhance the binding to p38α (ref. 34). Such molecular-level analysis, however, cannot determine whether ATP enhances binding at the docking site, phosphoacceptor binding to the P+1 site or both.

Therefore, in this study, we set out to clarify whether the docking interaction allosterically contributes to p38α activity. For this purpose, we prepared dually phosphorylated, active p38α (p38α-2P) and structurally analyzed its interaction with C-terminal fragments of MK2 containing both the docking sequence and the phosphoacceptor residue by solution NMR spectroscopy. We found that all of the individual steps in the p38α-2P kinase reaction, namely binding of ATP and phosphoacceptor residues to the p38α active site and subsequent phosphotransfer, are positively regulated by the docking interaction. Our findings clarify how MAPKs transduce signals steadily in the cell in various environments, including ATP-depleted conditions often associated with stresses, while distinguishing their specific substrates from other miscellaneous proteins.

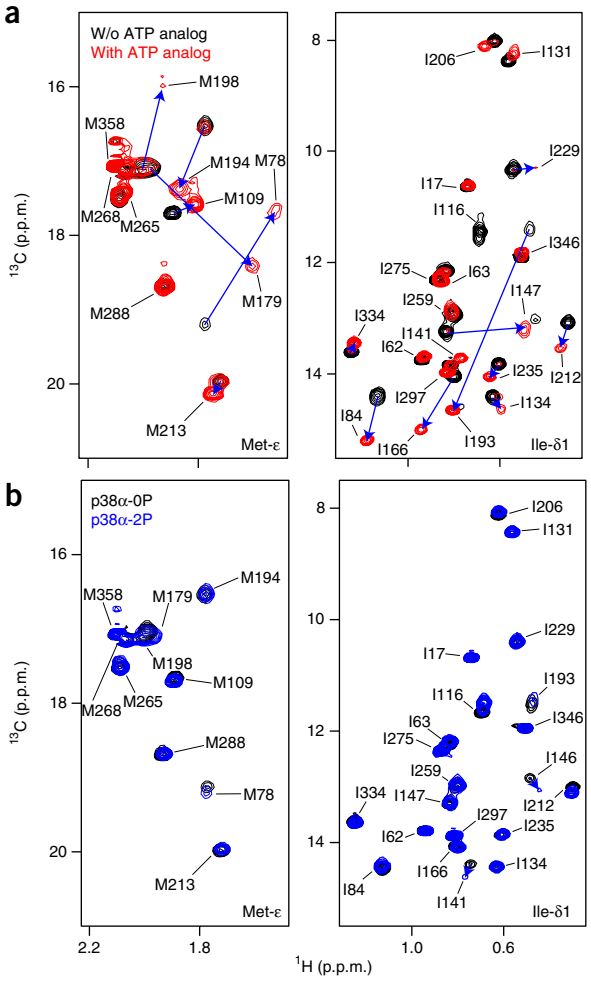

Figure 2 Effects of dual phosphorylation and ATP-analog binding on p38α NMR spectra. (**a**) Overlay of the annotated methionine and isoleucine (δ1) methyl ^{1}H-^{13}C band-selective optimized flip-angle short transient (SOFAST)-HMQC spectra of p38α-2P in the absence (black) and presence (red) of 5 mM ATP analog. Large chemical-shift changes are indicated by blue arrows. (**b**) Overlay of the annotated methionine and isoleucine (δ1) methyl ^{1}H-^{13}C SOFAST-HMQC spectra of p38α-2P (blue) and unphosphorylated p38α (black) in the apo state.

RESULTS

Phosphorylation- and ATP-induced p38α conformational change

As the first step toward gaining insight into the mechanistic regulation of substrate phosphorylation by p38α, we analyzed the phosphorylation- and ATP-dependent activation of p38α. We obtained dually phosphorylated, active p38α-2P by *in vitro* phosphorylation, using a constitutively active form of MAPKK6 (Online Methods and **Supplementary Fig. 1a–k**). p38α-2P in complex with ATP or an ATP analog (ATP-loaded p38α-2P) exhibited substantial chemical-shift perturbations (CSPs) in methyl ^{1}H-^{13}C heteronuclear multiple quantum correlation (HMQC) spectra, as compared to those of apo–p38α-2P (**Fig. 2a** and **Supplementary Fig. 2a**,**b**). Perturbed methyl sites were distributed throughout the structure of p38α and not localized to the ATP-binding site (**Fig. 3a**,**b** and **Supplementary Fig. 2b**), thus indicating

© 2014 Nature America, Inc. All rights reserved.

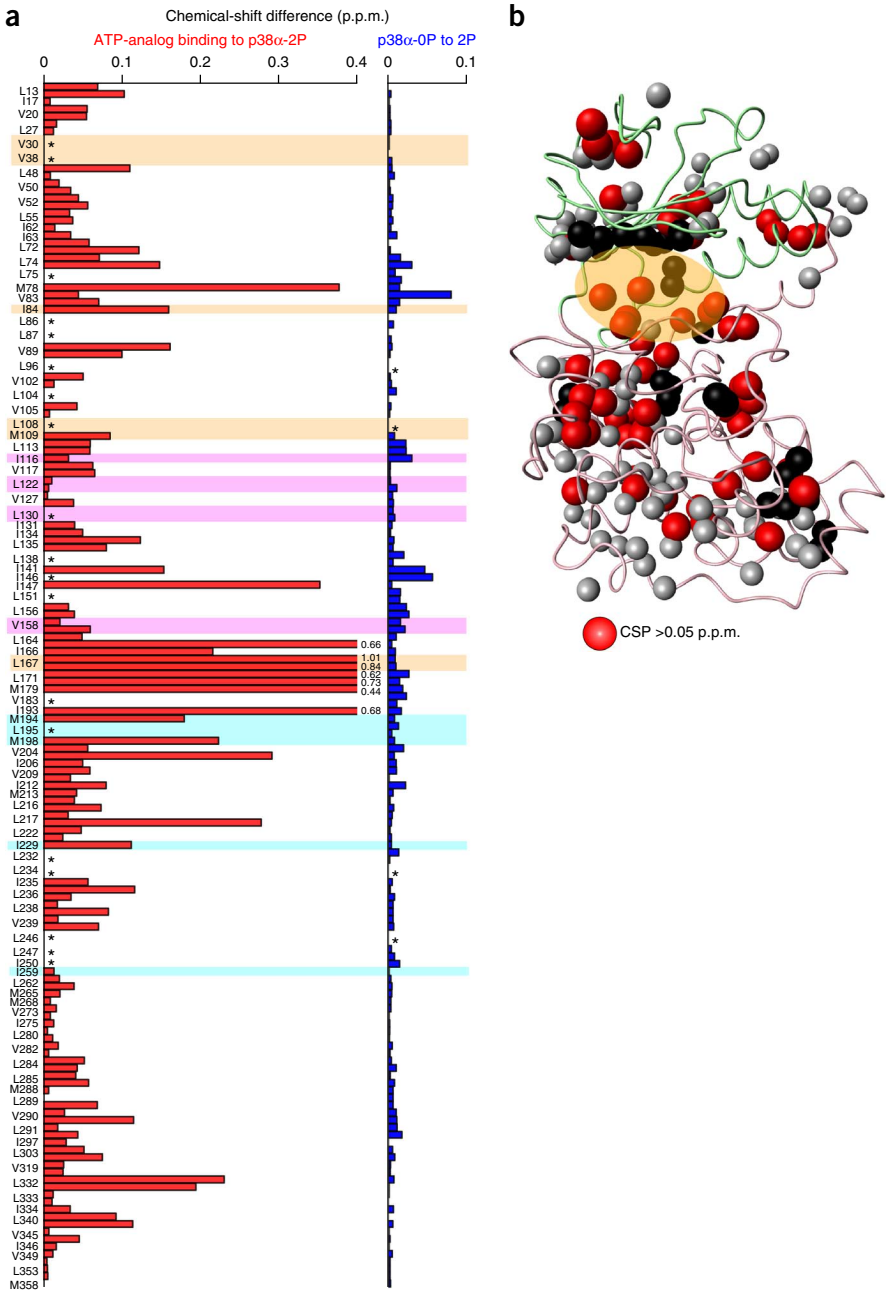

Figure 3 Chemical-shift changes induced by ATP-analog binding to p38α-2P and dual phosphorylation. (**a**) Bar graphs showing the methyl CSPs induced by ATP-analog binding to p38α-2P (left) and the chemical-shift differences between p38α-2P and unphosphorylated p38α (right). The residues in the ATP-binding, docking and P+1 sites are shaded in orange, magenta and cyan, respectively. Unassigned methyl sites are indicated by asterisks. CSP values larger than 0.4 p.p.m. are indicated. For leucine and valine, the values for δ1/γ1 are shown above the values for δ2/γ2. (**b**) Mapping of the CSPs induced by ATP-analog binding to p38α-2P (**a**, left) on the crystal structure of apo-p38α (PDB 1A9U[51]). ILVM-methyl groups are indicated as spheres, and those with CSPs larger than 0.05 p.p.m. are colored red. The ATP-binding site is highlighted by the orange oval. The structure is displayed in the same orientation as in **Figure 1a**.

that p38α underwent a conformational change to the active, closed state upon ATP binding, as observed in the crystal structure of p38γ-2P bound to AMP-PNP[18]. Interestingly, the spectral changes arising from the dual phosphorylation of p38α were smaller than those from ATP binding to p38α-2P (**Figs. 2b** and **3a** and **Supplementary Fig. 2c**). The only change apparent in the p38α spectrum upon dual phosphorylation was the disappearance of the amide ^{1}H-^{15}N resonances originating from the phosphorylated activation loop (aa 179–183), probably because of the conformational multiplicity of this region in the dually phosphorylated state (**Supplementary Fig. 3**). It should also be noted that we observed almost no spectral change for unphosphorylated p38α, even at a high concentration of ATP (4 mM; **Supplementary Fig. 2d**). Thus, both ATP binding and dual phosphorylation are essential to induce an active conformation of p38α-2P, and ATP binding appears to be more important for the overall structural change of p38α-2P, as indicated by the drastic spectral changes upon ATP binding (**Figs. 2** and **3**). In addition, the affinity of unphosphorylated p38α for ATP was quite weak (dissociation constant K_d >15 mM; **Supplementary Fig. 2e**). The size-exclusion chromatography (SEC) data also supported the ATP-dependent closure of p38α-2P, in which the elution volume of p38α-2P in the presence of ATP was larger than that in the absence of ATP (**Supplementary Fig. 1k**).

Substrate binding–induced CSPs in p38α

We next structurally investigated the interactions between the catalytically active, ATP-loaded p38α-2P and the model substrate, a 334D peptide (**Fig. 1b**). The 334D peptide, which contains the C-terminal unstructured region of the p38α substrate MK2, includes a native phosphorylation site, Thr334, and a C-terminal docking sequence. The K_d for 334D-peptide binding to p38α-2P was 80 nM, as determined by isothermal titration calorimetry, a value similar to that previously reported for the longer MK2 fragment (aa 47–400)[27]. Furthermore, the 334D peptide competed with the longer MK2 fragment for binding to p38α-2P (**Supplementary Fig. 1l**) and was phosphorylated more efficiently by p38α-2P than was the 334 peptide (**Supplementary Fig. 1m**), which lacks the docking sequence (**Fig. 1b**). These data confirmed that the 334D peptide retains the characteristics of native p38α substrates.

Titration of the unlabeled 334D peptide to p38α-2P, which was selectively labeled with ^{1}H and ^{13}C at methyl sites of isoleucine (δ1), leucine, valine and methionine (ILVM) residues, induced substantial spectral changes (**Figs. 4** and **5** and **Supplementary Fig. 4**). Resonances from the residues in the docking site, including Ile116 and Val158, exhibited substantial CSPs, both in the absence and presence of the ATP analog (**Fig. 5a–c**). We also observed a large CSP for Met109 in the hinge region, which is located above the docking site (**Fig. 5a–c**). This suggests that anchoring the substrate to p38α-2P via the docking interaction occurs independently of

© 2014 Nature America, Inc. All rights reserved.
npg

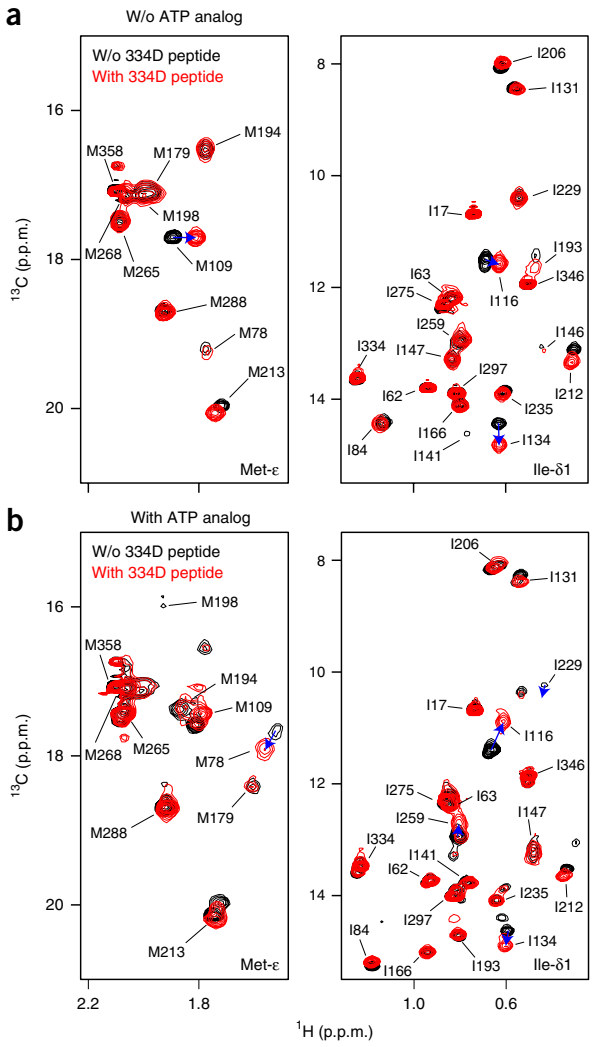

Figure 4 Effects of substrate binding on p38α NMR spectra. (**a**) Overlay of the annotated methionine and isoleucine (δ1) methyl ^{1}H-^{13}C SOFAST-HMQC spectra of p38α-2P without the ATP analog in the absence (black) and presence (red) of an equimolar amount of the 334D peptide. Large chemical-shift changes are indicated by blue arrows. (**b**) As in **a**, except that p38α-2P is in complex with the ATP analog.

ATP-analog binding. The spectral changes were saturated by the addition of an equimolar amount of the 334D peptide, indicating a tight 1:1 stoichiometric interaction between p38α-2P and the MK2 docking sequence (data not shown).

Interestingly, the resonances around the P+1 site showed distinct CSP patterns that were dependent on the presence of the ATP analog (**Fig. 5a–c**). As exemplified by the signals from Met194, Ile229 and Ile259, the P+1 site showed substantial CSPs only in the presence of the ATP analog. When the resonances from the ^{15}N-labeled 334D peptide were observed in the presence of unlabeled p38α-2P, addition of the ATP analog led to the disappearance of the resonances from the 334D peptide, including the resonance from the phosphoacceptor site, Thr334 (**Supplementary Fig. 5a**). These results indicate that the interaction of the 334D peptide with the P+1 site in p38α-2P is formed only upon ATP loading on p38α-2P. This characteristic was not specific to the ATP analog because it was also present for ATP (**Supplementary Fig. 5b**). Thus, the docking interaction itself is not sufficient to induce phosphoacceptor binding to the p38α-2P active site.

To investigate the direct interaction between the phosphoacceptor residues of the substrate and the active site of p38α-2P, we designed the 334 peptide, which consists of a 17-aa sequence centered at phospho acceptor Thr334 (**Fig. 1b**). In the absence of the ATP analog, the 334 peptide did not induce any spectral changes in p38α-2P, even when added in ten-fold molar excess (**Supplementary Fig. 5c**). In contrast, the P+1-site methyl resonances of p38α-2P exhibited CSPs and reduction of signal intensity only in the presence of the ATP analog (**Supplementary Fig. 5d**), a characteristic that was also present with ATP (**Supplementary Fig. 5e**). In addition, in titration of p38α-2P against the 334 peptide, we observed binding-induced line-broadening only in the presence of the ATP analog (**Supplementary Fig. 5f,g**). These results clearly show that the phosphoacceptor binds to the catalytic site only when ATP is loaded onto p38α-2P.

It should be noted that there were several residues outside the P+1 site that exhibited CSPs upon 334D-peptide titration that differed depending on ATP-analog presence (**Fig. 5a**). We found that binding of the ATP analog (**Fig. 2a**) and the 334D peptide (**Fig. 4a**) to the apo–p38α-2P induced similar CSPs of the residues in the allosteric site, thus offsetting the CSPs induced by the 334D peptide to ATP-loaded p38α-2P (**Fig. 4b**). In contrast, some residues showed larger CSPs in the presence of the ATP analog. Some of these residues (for example, Leu238 and Leu285) were located between the docking site and the P+1 site in the p38α structure; thus, the enhanced CSPs in the presence of the ATP analog might also reflect the phosphoacceptor binding to the P+1 site.

Docking-enhanced kinase-reaction steps of p38α-2P

The finding that the docking interaction does not guarantee binding of the phosphoacceptor residues to the p38α-2P active site also implied that the role of the docking interaction may be more complicated. Therefore, to investigate whether the docking interaction exerts allosteric effects on the p38α-2P active site, we titrated a D peptide, which contains only the docking sequence of MK2, against ILV methyl–labeled p38α-2P in the presence of the ATP analog (**Fig. 1b**). Interestingly, we observed CSPs for both the methyl resonances of the docking site and those of Val89 in the ATP-binding site and Ile259 near the P+1 site of p38α-2P (**Supplementary Fig. 6**), each of which is distant from the docking site of p38α-2P (**Fig. 1a**). Thus, these CSPs would reflect allosteric structural modifications to the active site induced by the D-peptide binding.

We determined the binding affinities of p38α-2P to ATP and to the ATP analog in the presence or absence of the D peptide. We determined the affinity for the ATP analog by measuring the dose-dependent decrease in the intensity of the unbound-state Ile84 signal in the ATP-binding site of p38α-2P (**Fig. 6a** and **Supplementary Fig. 7a**). We observed substantial enhancement of the affinity of p38α-2P for the ATP analog upon addition of the D peptide (**Table 1**). The affinity enhancement with the D peptide was more prominent for ATP (**Table 1** and **Supplementary Fig. 7b**).

We also investigated the allosteric effect in phosphoacceptor binding to the P+1 site of p38α-2P by determining the affinity of ATP-loaded p38α-2P for the 334 peptide. The dissociation constant decreased from 80 μM to 37 μM when the D peptide was present (**Fig. 6b**, **Table 1** and **Supplementary Fig. 7c**). Furthermore, the k_{cat} for phosphorylation of the 334 peptide by p38α-2P also increased upon addition of the D peptide (**Fig. 6c**, **Table 1** and **Supplementary Fig. 7d**).

© 2014 Nature America, Inc. All rights reserved.

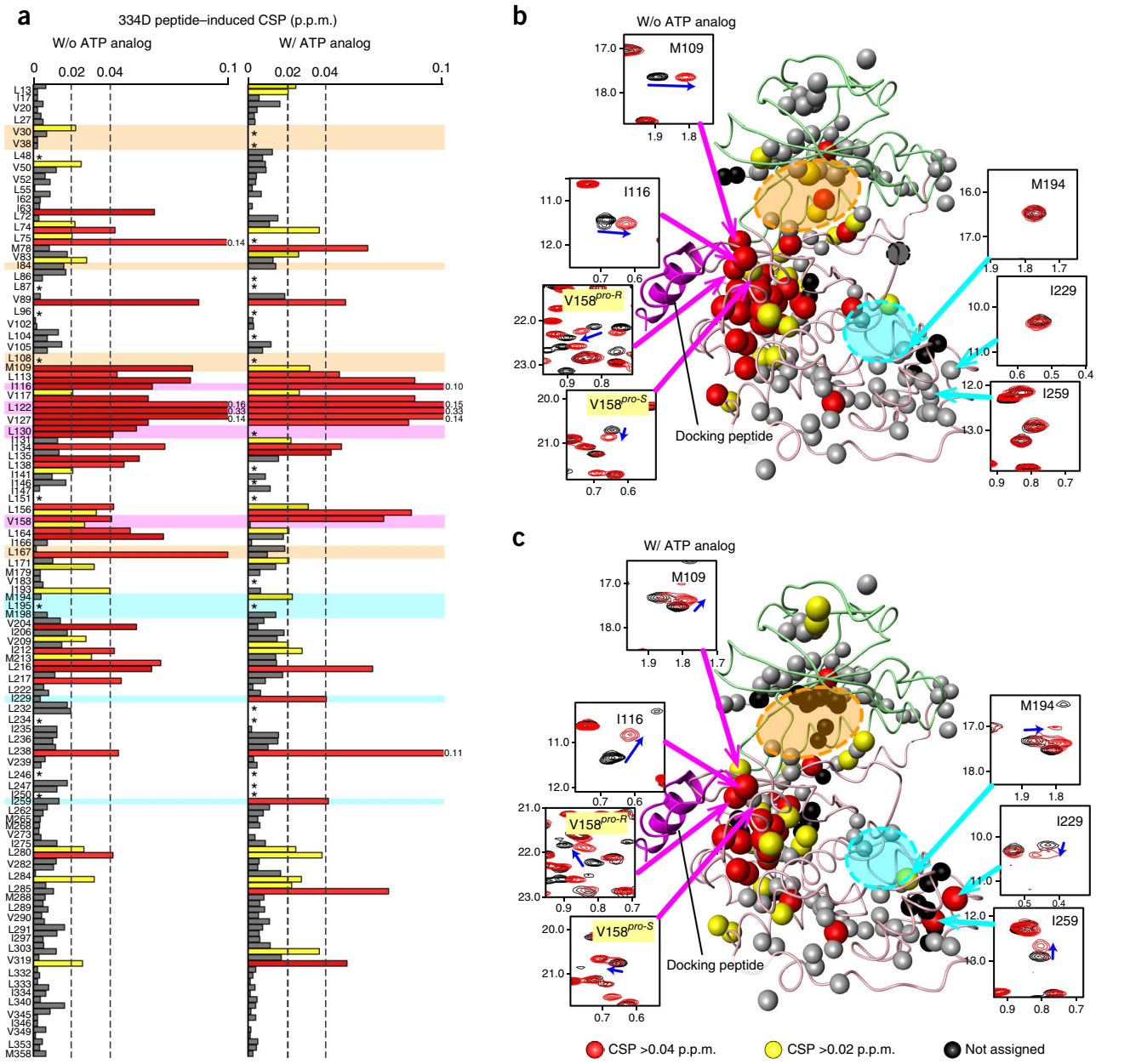

Figure 5 Site-resolved analyses of substrate binding to p38α-2P. (**a**) Bar graphs showing the methyl CSPs induced by 334D-peptide binding to p38α-2P in the absence (left) and presence (right) of the ATP analog. The residues in the ATP-binding, docking and P+1 sites are shaded in orange, magenta and cyan, respectively. Unassigned methyl sites are indicated by asterisks. CSP values larger than 0.1 p.p.m. are indicated. The CSPs at 0.02 p.p.m. and 0.04 p.p.m. are indicated by dashed gray lines. For leucine and valine, the values for δ1/γ1 are shown above the values for δ2/γ2. (**b**,**c**) Mapping of the CSPs induced by 334D-peptide binding on the crystal structure of p38α (PDB 2OKR[29]) without (**b**) and with (**c**) the ATP analog. The overlays of the ^{1}H-^{13}C spectral regions of selected methyl resonances of the hinge region (Met109), the docking sites (Ile116 and Val158) and the P+1 site (Met194, Ile229 and Ile259) are also indicated. ILVM-methyl groups that exhibited CSPs above 0.04 p.p.m. or 0.02 p.p.m. are represented as red and yellow spheres, respectively. Black spheres in **c** represent methyl groups with unassigned resonances in the 334D peptide–bound and/or the ATP analog–loaded p38α-2P. The ATP-binding and P+1 sites are indicated by orange and cyan ovals, respectively.

These results indicate that the docking interaction allosterically enhances the p38α-2P catalytic steps.

Although the high-affinity substrate MK2 forms a stable complex with p38α-2P, regardless of whether ATP is loaded on p38α-2P, other p38α substrates, such as myocyte enhancer factor 2A (MEF2A), have weaker docking affinities. For these substrates, ATP binding would occur before substrate docking. Thus, we also considered the case in which ATP is preloaded on p38α-2P. The titration of docking fragments from MEF2A and MK2 to p38α-2P in the absence or presence of the ATP analog revealed that preloading the ATP analog to p38α-2P considerably enhanced the affinity of the MEF2A docking sequence (**Supplementary Fig. 8a–d** and **Supplementary Table 1**), whereas the change in MK2 docking-sequence affinity was less substantial (**Supplementary Fig. 8e**,**f** and **Supplementary Table 1**). Thus, ATP binding and the docking interaction are mutually cooperative, and ATP preloading may contribute to specificity for substrates that dock more weakly.

© 2014 Nature America, Inc. All rights reserved.

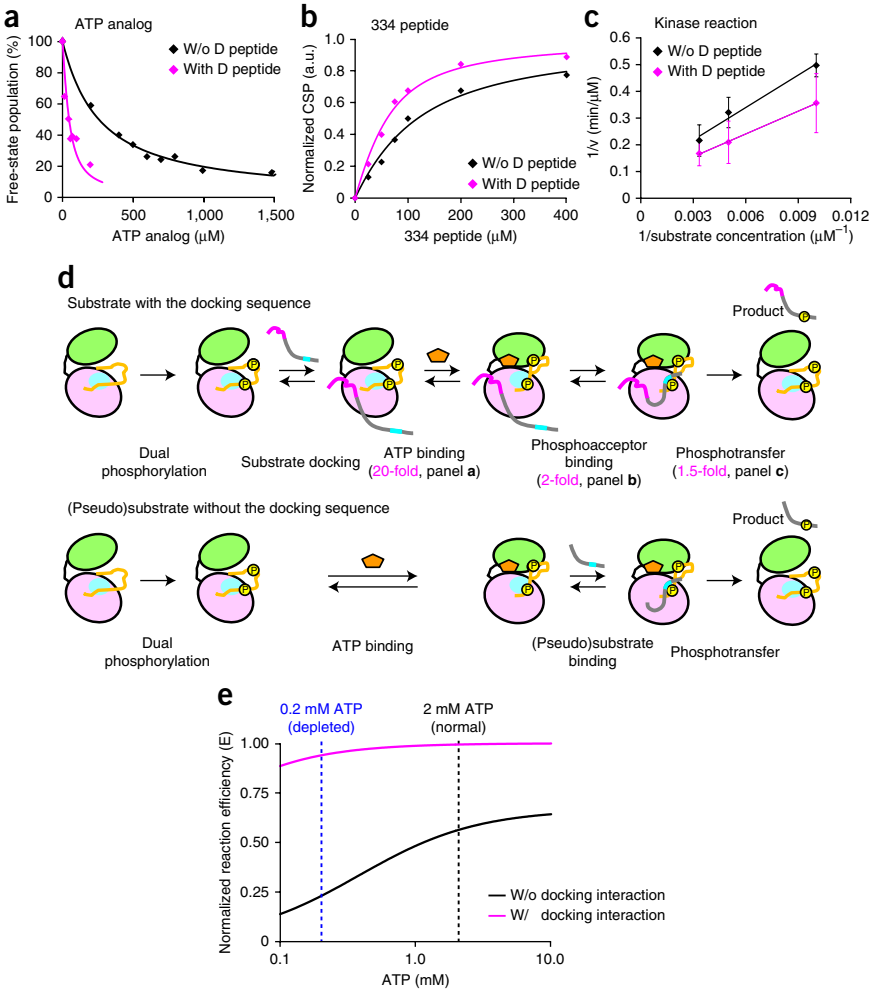

Figure 6 Allosteric positive modifications of p38α-2P kinase-reaction steps by the docking interaction. (**a**) ATP-unbound population of p38α-2P. (**b**) 334 peptide concentration–dependent, normalized CSPs of Ile259 resonances. a.u., arbitrary units. (**c**) Lineweaver-Burk plots of the phosphorylation of the 334 peptide by p38α-2P. Black and magenta lines in **a**–**c** represent data with and without the D peptide, respectively. For **a** and **b**, data representative of two independent experiments are shown. For **c**, error bars indicate the fitting errors of reaction velocities in independent experiments ($n = 3$). Experimental details are in Online Methods. (**d**) Schematic representation of p38α-2P kinase reaction process. As the initial step of activation, p38α is dually phosphorylated by the upstream MAPKKs (left). For genuine p38α substrates containing the docking sequence (top), p38α-2P recognizes the substrate via the docking interaction, binds ATP and then binds to the phosphoacceptor site of the substrate to lead to substrate phosphorylation. The docking-induced enhancements of the affinities and kinetics, in comparison to the (pseudo)substrate without the docking sequence (bottom) are indicated. Although omitted for clarification, ATP might bind before substrate docking. In that case, the affinities of the docking fragments to p38α-2P are enhanced by the ATP preloading (**Supplementary Table 1**). (**e**) ATP concentration dependence of the normalized reaction efficiencies (E) with (magenta) and without (black) formation of the docking interaction (details in Online Methods). ATP concentrations under the normal and the depleted conditions are indicated by the black and blue dashed lines, respectively.

DISCUSSION

Phosphorylation- and ATP-induced active conformation of p38α

In the previously reported crystal structures of dually phosphorylated MAPKs, both open and closed conformations have been observed[17–19,35]. Although it has been suggested that dual phosphorylation itself is sufficient to induce the conformational transition of ERK2, this notion is not consistent with the recent structures of ATP-unbound, dually phosphorylated p38α (refs. 19,35). In this study, we demonstrated that both dual phosphorylation and ATP binding are required to attain the active conformation of p38α-2P in solution (**Figs. 2** and **3** and **Supplementary Fig. 2**). This apparent difference in the requirement of ATP loading for the activating conformational transition may be due to different equilibria between the active and inactive conformations among MAPKs, or it may simply reflect the different crystallization conditions. Nevertheless, our NMR analyses clearly indicate that both dual phosphorylation and subsequent ATP loading are required for the full activation of p38α.

Table 1 Enhancements of substrate-phosphorylation steps of p38α-2P by the docking interaction

	Without D peptide	With D peptide	Enhancement ratio
K_d, ATP analog (μM)	209 ± 45[a]	17 ± 6.2[a]	12.3
K_d, ATP (μM)	381 ± 81[b]	13 ± 4.6[b]	29.3
K_d, 334 peptide (μM)	80 ± 13.0[a]	37 ± 1.5[a]	2.2
k_{cat} (/s)	17 ± 1.8[b]	24 ± 4.7[b]	1.4
K_m (μM)	420 ± 53[b]	410 ± 120[b]	1

[a]Difference between two individual experiments. [b]S.d. estimated from fitting errors.

Phosphoacceptor binding to p38α-2P requires ATP preloading

The NMR titration experiments of the 334D peptide against p38α-2P and separately observed docking and phosphoacceptor interactions clearly demonstrated that the phosphoacceptor residue binds to the P+1 site only when ATP is loaded on p38α-2P, whereas the docking interaction is spontaneous and does not require ATP loading (**Fig. 5b**,**c**). ATP binding to p38α-2P seems to be central for induction of the active conformation of the P+1 site because it enhances the interaction between the N and C lobes via the activation loop, which directly precedes the P+1 site in the amino acid sequence. ATP binding before phosphoacceptor binding seems to be structurally preferable because the ATP-binding site is located deep in the cleft between the N and C lobes, whereas the P+1 site is located outside the ATP-binding pocket. Thus, a random or inverted order may interfere with the ATP loading on p38α-2P and may prevent efficient phosphotransfer.

Kinase-reaction steps optimized by the docking interaction

We found that binding of the MK2 docking sequence to p38α-2P positively regulates each individual step in the kinase reaction: ATP loading, phosphoacceptor binding and the subsequent phosphotransfer reaction (**Fig. 6**). The affinity of p38α-2P for ATP also increased more than one order of magnitude in the presence of docking fragments derived from other p38α substrates, MEF2A and ATF2

© 2014 Nature America, Inc. All rights reserved.

(data not shown). Thus, the enhancement of the kinase reaction from formation of docking interactions with physiological substrates seems to be a conserved characteristic of p38α. The DEF motif, another type of docking sequence identified in many ERK1/2 substrates and consisting of a consensus sequence of FXFP[36], however, is beyond the scope of this study. Dalby and co-workers reported that the deletion of the N-terminal docking sequence of the transcription factor Ets-1 does not influence the k_{cat} of ERK2 (ref. 37); however, Ets-1 has a SAM domain that binds the FXFP site in addition to the N-terminal docking sequence. Veglia and co-workers reported that binding of either AMP-PNP or a phosphoacceptor peptide, kemptide, allosterically enhances subsequent binding of the other to the active site of protein kinase A for efficient substrate phosphorylation[38]. Our findings are distinct from the former study, showing the collaborative interplay between the kinase reaction and the docking interaction, the latter of which occurs outside the active site and represents a key element for specific substrate recognition. Thus, the allosteric enhancement of the kinase reaction by the docking interaction, shown here, couples specific substrate recognition to efficient phosphorylation, thereby providing a rationale for the strict selectivity of the MAPK pathway in the cellular context.

Biological importance of the elucidated mechanism

In the intracellular environment, many macromolecules such as proteins and nucleic acids exist at concentrations up to 300 mg/ml (ref. 39). Under such dense conditions, random collisions and nonspecific interactions between the macromolecules are expected to be common. Even under such chaotic conditions, biomolecules use multiple specific interactions and reactions to maintain cellular homeostasis and environmental responsiveness. The p38α MAPK cascade is a well-known representative of this strictly controlled signal-transduction pathway. The fine-tuned coupling between the enzymatic reaction and the specific docking interaction, shown here, may maximize the reaction efficiency for a substrate that has both the docking sequence and phosphoacceptor residues in the same polypeptide chain (**Fig. 6d**). We found that the docking interaction induces enhanced affinity for the substrate phosphoacceptor site and for ATP, corresponding to a free-energy gain of −0.4 kcal/mol and −1.8 kcal/mol, respectively. Thus, in total, the docking interaction contributes −2.2 kcal/mol energetic gain, favoring formation of the functional trimeric complex. Although the energetic gain for phosphoacceptor binding is less than that for ATP binding, the stabilization of both elements is required to enhance the formation of the functional trimeric p38α-2P–ATP–phosphoacceptor complex. In addition, the docking interaction enhanced k_{cat}. Therefore, the kinase activity of p38α toward nonspecific targets or pseudosubstrates without a docking sequence, both of which would be abundant in the cell given the simple consensus phosphoacceptor motif of MAPKs, is maintained at a very low level to avoid undesired phosphorylations and to conserve the cellular energy source, ATP (**Fig. 6d**). The mechanism diverts the specific p38α pathway, which relies on the docking interaction, from other unwanted random events so that it may appropriately integrate environmental inputs to evoke the necessary cellular responses.

Aberrant activation of protein kinases can result in fatal diseases such as cancer[40,41]. Thus, many kinases have regulatory domains that enable specific activation by certain signals and suppress activity when it is not necessary[21]. MAPKs, however, are composed of only a catalytic domain and therefore require another regulatory mechanism. The modulation of kinase activity by the docking interaction may fulfill this need. Allosteric regulation by the docking interaction seems to be reasonable, considering that p38α is the molecular hub in the MAPK cascade and must interact with several upstream and downstream molecules that belong to the same signaling cascade. Regulatory domains often exhibit very precise selectivity to certain molecules, and they might be too selective to act as molecular hubs. Thus, the docking interaction seems to provide a good balance between the requirements for both specificity and robustness of the MAPK signal. For some authentic p38α substrates lacking any docking sequences, another mechanism, such as subcellular colocalization, may operate to ensure efficient phosphorylation *in vivo*[6].

One of the most intriguing findings in this study is the affinity enhancement of p38α-2P for ATP by the docking interaction (**Fig. 6a** and **Supplementary Fig. 7a**,**b**). Most protein kinases have an apparent Michaelis constant for ATP of less than 50 μM (refs. 42,43), and such kinetics may have been evolutionarily optimized for kinases to work properly in cellular environments. The affinity of p38α-2P for ATP in the absence of the docking interaction (430 μM) is atypically weak. Although cells maintain the homeostatic ATP concentration at 1–2 mM under normal conditions, intracellular ATP concentrations can drop in certain physiological conditions that require p38α activation. For example, in the ischemic heart, the ATP concentration can be as low as 20% of the normal level[44]. Additionally, ATP concentration reportedly drops in response to UV exposure and cellular senescence[45]. Even under these ATP-depleted conditions, p38α is required to transfer stress signals[46]. The enhancement of the ATP binding affinity by the docking interaction may contribute to p38α function during stress, as shown in the simulated ATP-concentration dependence of the substrate phosphorylation efficiency by p38α (**Fig. 6e**). Thus, the allosteric regulation of p38α-2P by the docking interaction seems to be physiologically important, especially in stress-response signaling.

Although previous studies have used NMR to investigate the function and interactions of p38α (refs. 47–49), to our knowledge, our study is the first to clarify and quantify the allosteric enhancement of p38α enzymatic activity by the docking interaction. We emphasize that the observations presented here are based on firm experimental evidence using the dually phosphorylated, enzymatically active p38α. In addition, the advantage of solution NMR in providing structural information under nearly physiological conditions was crucial to revealing the structural basis for allosteric regulation.

We have shown that phosphoacceptor binding to the active site of p38α-2P requires ATP binding and that the docking interaction alone is not sufficient for the phosphoacceptor residue to bind to the active site of p38α-2P. Furthermore, the docking interaction allosterically enhances p38α-2P enzymatic function. Such regulatory mechanisms may help p38α effectively phosphorylate its specific substrates, even under low cellular ATP concentrations, while avoiding the nonspecific phosphorylation of random kinase substrates in the cell.

Given that the docking interaction is a conserved characteristic of the interactions between MAPKs and their partners, the roles of the docking interactions in other MAPKs must also be considered. In addition, there are many other examples in which the specific interactions between enzymes and substrates are distant from the catalytic cores[21]. Although it is clear that these interactions contribute to maximizing the encounter rate between the enzymes and their substrates, the possible contribution of an allosteric enhancement should also be considered.

METHODS

Methods and any associated references are available in the online version of the paper.

© 2014 Nature America, Inc. All rights reserved.

Accession codes. Methyl resonance assignments have been deposited in the Biological Magnetic Resonance Data Bank under accession codes 19930 (nonphosphorylated apo-p38α), 19934 (apo–p38α-2P), 19935 (p38α-2P in ATP analog–bound state), 19936 (p38α-2P in 334D peptide–bound state) and 19937 (p38α-2P in both ATP analog– and substrate-bound states).

Note: Any Supplementary Information and Source Data files are available in the online version of the paper.

ACKNOWLEDGMENTS

We would like to thank H. Hanzawa (Daiichi Sankyo Co.) for providing the expression plasmid for p38α. We are also indebted to N. Goshima (Japanese National Institute of Advanced Industrial Science and Technology) for providing cDNA clones for the phosphatases PPM1A and HePTP. This work was funded by grants from the Japan New Energy and Industrial Technology Development Organization (NEDO). Funding was also provided by Grants-in-Aid for Scientific Research on Innovative Areas (25121743 to K.T.) from the Japanese Ministry of Education, Culture, Sports, Science and Technology (MEXT) and Japan Society for the Promotion of Science (JSPS).

AUTHOR CONTRIBUTIONS

Y.T., K.T., H.T. and I.S. conceived the project. Y.T. performed the experiments. Y.T., K.T., H.T. and I.S. wrote the manuscript.

COMPETING FINANCIAL INTERESTS

The authors declare no competing financial interests.

Reprints and permissions information is available online at http://www.nature.com/reprints/index.html.

1. Raman, M., Chen, W. & Cobb, M.H. Differential regulation and properties of MAPKs. *Oncogene* **26**, 3100–3112 (2007).
2. Avruch, J. MAP kinase pathways: the first twenty years. *Biochim. Biophys. Acta* **1773**, 1150–1160 (2007).
3. Cargnello, M. & Roux, P.P. Activation and function of the MAPKs and their substrates, the MAPK-activated protein kinases. *Microbiol. Mol. Biol. Rev.* **75**, 50–83 (2011).
4. Plotnikov, A., Zehorai, E., Procaccia, S. & Seger, R. The MAPK cascades: signaling components, nuclear roles and mechanisms of nuclear translocation. *Biochim. Biophys. Acta* **1813**, 1619–1633 (2011).
5. Marshall, C.J. Specificity of receptor tyrosine kinase signaling: transient versus sustained extracellular signal-regulated kinase activation. *Cell* **80**, 179–185 (1995).
6. Cuadrado, A. & Nebreda, A.R. Mechanisms and functions of p38 MAPK signalling. *Biochem. J.* **429**, 403–417 (2010).
7. Schindler, J.F., Monahan, J.B. & Smith, W.G. p38 pathway kinases as anti-inflammatory drug targets. *J. Dent. Res.* **86**, 800–811 (2007).
8. Dodeller, F. & Schulze-Koops, H. The p38 mitogen-activated protein kinase signaling cascade in CD4 T cells. *Arthritis Res. Ther.* **8**, 205 (2006).
9. Johnson, G.L. & Lapadat, R. Mitogen-activated protein kinase pathways mediated by ERK, JNK, and p38 protein kinases. *Science* **298**, 1911–1912 (2002).
10. Anderson, N.G., Maller, J.L., Tonks, N.K. & Sturgill, T.W. Requirement for integration of signals from two distinct phosphorylation pathways for activation of MAP kinase. *Nature* **343**, 651–653 (1990).
11. Zhang, Y.Y., Mei, Z.Q., Wu, J.W. & Wang, Z.X. Enzymatic activity and substrate specificity of mitogen-activated protein kinase p38α in different phosphorylation states. *J. Biol. Chem.* **283**, 26591–26601 (2008).
12. Keyse, S.M. Protein phosphatases and the regulation of mitogen-activated protein kinase signalling. *Curr. Opin. Cell Biol.* **12**, 186–192 (2000).
13. Goldsmith, E.J., Cobb, M.H. & Chang, C.I. Structure of MAPKs. *Methods Mol. Biol.* **250**, 127–144 (2004).
14. Wang, Z. *et al.* The structure of mitogen-activated protein kinase p38 at 2.1-A resolution. *Proc. Natl. Acad. Sci. USA* **94**, 2327–2332 (1997).
15. Wilson, K.P. *et al.* Crystal structure of p38 mitogen-activated protein kinase. *J. Biol. Chem.* **271**, 27696–27700 (1996).
16. Zhang, F., Strand, A., Robbins, D., Cobb, M. & Goldsmith, E. Atomic structure of the MAP kinase ERK2 at 2.3 A resolution. *Nature* **367**, 704–711 (1994).
17. Bellon, S., Fitzgibbon, M.J., Fox, T., Hsiao, H.M. & Wilson, K.P. The structure of phosphorylated p38γ is monomeric and reveals a conserved activation-loop conformation. *Structure* **7**, 1057–1065 (1999).
18. Canagarajah, B.J., Khokhlatchev, A., Cobb, M.H. & Goldsmith, E.J. Activation mechanism of the MAP kinase ERK2 by dual phosphorylation. *Cell* **90**, 859–869 (1997).
19. Zhang, Y.Y., Wu, J.W. & Wang, Z.X. Mitogen-activated protein kinase (MAPK) phosphatase 3-mediated cross-talk between MAPKs ERK2 and p38α. *J. Biol. Chem.* **286**, 16150–16162 (2011).
20. Weston, C.R., Lambright, D.G. & Davis, R.J. Signal transduction. MAP kinase signaling specificity. *Science* **296**, 2345–2347 (2002).
21. Ubersax, J.A. & Ferrell, J.E. Mechanisms of specificity in protein phosphorylation. *Nat. Rev. Mol. Cell Biol.* **8**, 530–541 (2007).
22. Tanoue, T. & Nishida, E. Docking interactions in the mitogen-activated protein kinase cascades. *Pharmacol. Ther.* **93**, 193–202 (2002).
23. Tanoue, T., Adachi, M., Moriguchi, T. & Nishida, E. A conserved docking motif in MAP kinases common to substrates, activators and regulators. *Nat. Cell Biol.* **2**, 110–116 (2000).
24. Gupta, S., Campbell, D., Derijard, B. & Davis, R.J. Transcription factor ATF2 regulation by the JNK signal transduction pathway. *Science* **267**, 389–393 (1995).
25. Kallunki, T. *et al.* JNK2 contains a specificity-determining region responsible for efficient c-Jun binding and phosphorylation. *Genes Dev.* **8**, 2996–3007 (1994).
26. Yang, S.-H., Galanis, A. & Sharrocks, A.D. Targeting of p38 mitogen-activated protein kinases to MEF2 transcription factors. *Mol. Cell. Biol.* **19**, 4028–4038 (1999).
27. Lukas, S.M. *et al.* Catalysis and function of the p38α-MK2a signaling complex. *Biochemistry* **43**, 9950–9960 (2004).
28. Chang, C.I., Xu, B.E., Akella, R., Cobb, M.H. & Goldsmith, E.J. Crystal structures of MAP kinase p38 complexed to the docking sites on its nuclear substrate MEF2A and activator MKK3b. *Mol. Cell* **9**, 1241–1249 (2002).
29. ter Haar, E., Prabhakar, P., Prabakhar, P., Liu, X. & Lepre, C. Crystal structure of the p38α-MAPKAP kinase 2 heterodimer. *J. Biol. Chem.* **282**, 9733–9739 (2007).
30. Tanoue, T., Maeda, R., Adachi, M. & Nishida, E. Identification of a docking groove on ERK and p38 MAP kinases that regulates the specificity of docking interactions. *EMBO J.* **20**, 466–479 (2001).
31. Reményi, A., Good, M.C., Bhattacharyya, R.P. & Lim, W.A. The role of docking interactions in mediating signaling input, output, and discrimination in the yeast MAPK network. *Mol. Cell* **20**, 951–962 (2005).
32. Songyang, Z. *et al.* A structural basis for substrate specificities of protein Ser/Thr kinases: primary sequence preference of casein kinases I and II, NIMA, phosphorylase kinase, calmodulin-dependent kinase II, CDK5, and Erk1. *Mol. Cell. Biol.* **16**, 6486–6493 (1996).
33. White, A., Pargellis, C.A., Studts, J.M., Werneburg, B.G. & Farmer, B.T. Molecular basis of MAPK-activated protein kinase 2:p38 assembly. *Proc. Natl. Acad. Sci. USA* **104**, 6353–6358 (2007).
34. Szafranska, A.E. & Dalby, K.N. Kinetic mechanism for p38 MAP kinase α. *FEBS J.* **272**, 4631–4645 (2005).
35. Akella, R., Min, X., Wu, Q., Gardner, K.H. & Goldsmith, E.J. The third conformation of p38α MAP kinase observed in phosphorylated p38α and in solution. *Structure* **18**, 1571–1578 (2010).
36. Jacobs, D., Glossip, D., Xing, H., Muslin, A.J. & Kornfeld, K. Multiple docking sites on substrate proteins form a modular system that mediates recognition by ERK MAP kinase. *Genes Dev.* **13**, 163–175 (1999).
37. Lee, S. *et al.* A model of a MAPKsubstrate complex in an active conformation: a computational and experimental approach. *PLoS ONE* **6**, e18594 (2011).
38. Masterson, L.R., Mascioni, A., Traaseth, N.J., Taylor, S.S. & Veglia, G. Allosteric cooperativity in protein kinase A. *Proc. Natl. Acad. Sci. USA* **105**, 506–511 (2008).
39. Zimmerman, S.B. & Trach, S.O. Estimation of macromolecule concentrations and excluded volume effects for the cytoplasm of *Escherichia coli*. *J. Mol. Biol.* **222**, 599–620 (1991).
40. Lugo, T.G., Pendergast, A.M., Muller, A.J. & Witte, O.N. Tyrosine kinase activity and transformation potency of bcr-abl oncogene products. *Science* **247**, 1079–1082 (1990).
41. Heisterkamp, N. *et al.* Acute leukaemia in *bcr/abl* transgenic mice. *Nature* **344**, 251–253 (1990).
42. Dennis, P.B. *et al.* Mammalian TOR: a homeostatic ATP sensor. *Science* **294**, 1102–1105 (2001).
43. Knight, Z.A. & Shokat, K.M. Features of selective kinase inhibitors. *Chem. Biol.* **12**, 621–637 (2005).
44. Steenbergen, C., Murphy, E., Watts, J.A. & London, R.E. Correlation between cytosolic free calcium, contracture, ATP, and irreversible ischemic injury in perfused rat heart. *Circ. Res.* **66**, 135–146 (1990).
45. Schütt, F., Aretz, S., Auffarth, G.U. & Kopitz, J. Moderately reduced ATP levels promote oxidative stress and debilitate autophagic and phagocytic capacities in human RPE cells. *Invest. Ophthalmol. Vis. Sci.* **53**, 5354–5361 (2012).
46. Kumphune, S., Chattipakorn, S. & Chattipakorn, N. Role of p38 inhibition in cardiac ischemia/reperfusion injury. *Eur. J. Clin. Pharmacol.* **68**, 513–524 (2012).
47. Nielsen, G. & Schwalbe, H. NMR spectroscopic investigations of the activated p38α mitogen-activated protein kinase. *ChemBioChem* **12**, 2599–2607 (2011).
48. Francis, D.M. *et al.* Structural basis of p38α regulation by hematopoietic tyrosine phosphatase. *Nat. Chem. Biol.* **7**, 916–924 (2011).
49. Piserchio, A. *et al.* Docking interactions of hematopoietic tyrosine phosphatase with MAP kinases ERK2 and p38α. *Biochemistry* **51**, 8047–8049 (2012).
50. Arnold, K., Bordoli, L., Kopp, J. & Schwede, T. The SWISS-MODEL workspace: a web-based environment for protein structure homology modelling. *Bioinformatics* **22**, 195–201 (2006).
51. Wang, Z. *et al.* Structural basis of inhibitor selectivity in MAP kinases. *Structure* **6**, 1117–1128 (1998).

© 2014 Nature America, Inc. All rights reserved.

ONLINE METHODS

Preparation of unphosphorylated p38α. The pET15b vector for the expression of human p38α (aa 2–360) with an N-terminal hexahistidine (His_6) tag was a kind gift from H. Hanzawa (Daiichi Sankyo Co.). The *Escherichia coli* BL21 (DE3) transformed with the plasmid was grown in 10 mL of Luria-Bertani (LB) medium containing 100 mg/mL ampicillin, at 37 °C overnight. The cells were further inoculated into 1 l of D_2O-based ampicillin-M9 medium supplemented with D-[$^2H_7$/$^{13}C_6$]glucose and $^{15}NH_4Cl$ as the sole carbon and nitrogen sources, respectively. When the culture attained an optical density at a wavelength of 600 nm (OD_{600}) of 0.6, 0.5 mM isopropyl-β-D-thiogalactopyranoside (IPTG) was added to induce protein expression. The culture was further incubated at 16 °C for 16 h. For selective $^{13}CH_3$ labeling of the isoleucine (δ1), leucine, valine and methionine methyl groups in a $^2H/^{12}C$ background (so-called ILVM-methyl labeling[52,53]), 70 mg/L of [methyl-^{13}C, 3,3-$^2H_2$]α-ketobutyric acid, 100 mg/L of [3-methyl-^{13}C, 3,4,4,4-$^2H_4$]α-ketoisovaleric acid and 50 mg/L of L-[methyl-^{13}C]methionine were supplemented into the medium, 30 min before the addition of IPTG. The p38α was purified from the supernatant of the cell lysate by two column-chromatography steps, including nickel affinity and SEC. The cell lysate was applied to an Ni-NTA agarose (Qiagen) column equilibrated with a buffer consisting of 20 mM Tris-HCl, pH 8.0, 500 mM NaCl, 2 mM dithiothreitol (DTT), 10 mM imidazole and 0.6% (w/v) CHAPS. After thorough washing of the column with the equilibration buffer, p38α was eluted with the same buffer but containing 250 mM imidazole. The eluate was further purified by SEC, with a HiLoad Superdex 200 prep-grade column (GE Healthcare), which was equilibrated with a buffer containing 50 mM NaPi, pH 6.8, 150 mM NaCl and 3 mM DTT. The eluate fraction was buffer-exchanged into 25 mM Tris-HCl, pH 7.5, with 150 mM NaCl and 5 mM DTT and stored at −30 °C until use.

Preparation of the constitutively active MAPKK6. The cDNA clone of human MAPKK6 (MKK6) was purchased from Toyobo. MKK6 (aa 1–334) was subcloned into the pGEX-5X-3 vector with an N-terminal glutathione S-transferase (GST) tag followed by a factor Xa cleavage site. The constitutively active S207D T211D MKK6 mutant ($MKK6^{DD}$) was constructed with a QuikChange Mutagenesis Kit (Agilent Technologies). BL21 (DE3) cells transformed with the plasmid were grown in LB medium. When the culture attained an OD_{600} of 0.6, 0.5 mM IPTG was added to induce protein expression. The culture was then incubated at 16 °C for 20 h. The $MKK6^{DD}$ protein was purified by GST-affinity chromatography. Briefly, the cells, resuspended in 50 mL of buffer (10 mM Tris-HCl, pH 8.0, 100 mM NaCl, 1 mM EDTA and 10% (w/v) glycerol), were lysed by sonication. Triton X-100 and DTT were added to final concentrations of 1% (w/v) and 2 mM, respectively. The lysate was incubated at 4 °C for 30 min with rotation. The supernatant was applied to a glutathione Sepharose 4B column (GE Healthcare). After the column was thoroughly washed, $MKK6^{DD}$ was eluted with buffer containing 25 mM Tris-HCl, pH 7.4, 150 mM NaCl, 2 mM DTT and 50 mM reduced glutathione. The eluate was buffer-exchanged by dialysis against 1 l of storage buffer, containing 25 mM Tris-HCl, pH 7.5, 150 mM NaCl, 2 mM DTT and 10% (w/v) glycerol. The resulting stock was stored on ice, and its activity was retained for at least six months.

Preparation of the p38α substrate, MK2. The full-length cDNA clone of human MK2 was purchased from Toyobo. From the MK2 cDNA, four fragments corresponding to aa 47–400, 326–400 (334D peptide), 326–342 (334 peptide) and 369–400 (D peptide) were amplified by polymerase chain reaction (PCR) (**Fig. 1b**). The longer MK2 fragment (aa 47–400) was ligated into the pET15b vector with an N-terminal His_6 tag. The smaller MK2 fragments were ligated into the pET28a vector with an N-terminal GB1 tag followed by a human rhinovirus 3C (HRV3C) cleavage site and a C-terminal His_6 tag. These plasmids were transformed into BL21 (DE3) for protein expression. The bacterial culture for the D peptide was grown in LB medium, whereas cultures for MK2, the 334D peptide and the 334 peptide were grown in M9 medium. When the cultures reached an OD_{600} of 0.6, the medium was supplemented with 1 mM IPTG, and the cultures were then incubated at 25 °C for 12 h. The longer MK2 fragment was purified with a four-step column-chromatography procedure according to the previously reported protocol[54], with minor modifications. The 334D, 334 and D peptides were purified by nickel-affinity chromatography. The GB1 tag was removed from the D peptide by HRV3C protease and then separated from HRV3C and GB1 by nickel-affinity chromatography.

Preparation of dually phosphorylated p38α (p38α-2P). Unphosphorylated p38α (10 μM) was phosphorylated by a 0.014 molar equivalent of $MKK6^{DD}$, in a reaction buffer containing 50 mM Tris-HCl, pH 8.0, 100 mM NaCl, 2 mM DTT, 10 mM $MgCl_2$, 0.5 mM EDTA and 2 mM ATP, by following a previously published protocol with minor modifications[11]. The reaction was carried out at 14 °C for 48 h. The completion of the dual-phosphorylation reaction was confirmed by SDS-PAGE, with a 9% polyacrylamide gel supplemented with 30 μM of Phos-tag acrylamide[55] (**Supplementary Fig. 1a**), as well as by NMR (**Supplementary Fig. 1b–i**). p38α-2P was isolated from $MKK6^{DD}$ by nickel-affinity chromatography. The kinase activity of the prepared p38α-2P was measured by an *in vitro* kinase assay at 25 °C with MK2 as the substrate. The reaction mixture consisted of 5 μM MK2 and 0.5 μM p38α-2P, in the same buffer used for the phosphorylation of p38α by $MKK6^{DD}$. Phosphorylation of MK2 was confirmed by Phos-tag SDS-PAGE (**Supplementary Fig. 1j**). The active p38α-2P was used for further analysis.

NMR experiments. Vogtherr *et al.*[56] reported that 25% of the backbone-amide ^1H-^{15}N resonances in the unphosphorylated p38α were not observed, probably because of local conformational multiplicities, and 36% of the backbone resonances were not assigned. The unobservable/unassigned regions contain the residues in the ATP-binding site and a large part of the phosphoacceptor-binding site. Therefore, we used the methyl-TROSY technique[57] to obtain the structural information for these sites. Methyl $^1H/^{13}C$ resonances are highly sensitive in a uniformly deuterated background and thus provide high-quality NMR spectra. The ILVM-methyl moieties of p38α were selectively $^1H/^{13}C$-labeled with established protocols[58].

Uniformly $^2H/^{13}C/^{15}N$-labeled p38α-2P was concentrated to 0.1–0.4 mM in 220 μL of aqueous buffer containing 25 mM Tris-HCl, pH 7.5, 150 mM NaCl, 5 mM DTT and 10% D_2O. NMR samples of ILVM (or ILV) methyl–labeled p38α-2P were prepared in D_2O-based buffer at protein concentrations of 20 μM and 40 μM for two-dimensional (2D) experiments and 0.3 mM for three-dimensional (3D) experiments. For the analysis of p38α-2P in the presence of ATP or analogous compounds such as ADP, 5′-adenylyl imidodiphosphate (AMP-PNP), adenylyl methylenediphosphate (AMP-PCP), ATP-γS and AMP, the buffer was supplemented with 20 mM $MgCl_2$. We found that p38α-2P has intrinsic ATPase activity, and more than 50% of 1 mM ATP was hydrolyzed in 30 min at 25 °C in the presence of 20 μM p38α-2P (data not shown). To avoid chemical inhomogeneity due to ATP hydrolysis by p38α-2P, we used ADP as an ATP analog unless otherwise indicated. ADP had almost the same affinity for p38α-2P as did ATP, and the NMR spectrum of the ADP-bound p38α-2P closely matched that of the ATP-loaded p38α-2P (data not shown). The NMR spectra of p38α-2P in complex with other conventional ATP analogs, such as AMP-PNP, AMP-PCP and ATP-γS, did not fully reproduce the spectrum with ATP. Thus, we chose ADP as the most appropriate ATP analog for this study. To obtain the ATP-bound p38α-2P spectra, the experimental time was shortened with a ^1H-^{13}C SOFAST-HMQC experiment[59] and the highest-field magnet (800 MHz in ^1H frequency) equipped with a TCI cryoprobe. Experiments were conducted at a low temperature (10 °C) to minimize ATP hydrolysis. Under these conditions, the ATP hydrolysis during the experiment was suppressed to less than 10%, as confirmed by the ^1H-1D spectra before and after the SOFAST-HMQC measurement. For kinetic analyses of 334-peptide phosphorylation, a buffer consisting of 50 mM Tris-HCl, pH 8.0, 100 mM NaCl, 2 mM DTT, 0.5 mM EDTA, 10 mM $MgCl_2$ and 10% D_2O was used. All NMR spectra were measured at 600, 700 and 800 MHz ^1H frequencies on Bruker Avance spectrometers equipped with a TXI cryoprobe, a TXI room-temperature probe and a TCI cryoprobe, respectively. All NMR experiments were performed at 25 °C, except for the ^1H-^{13}C SOFAST-HMQC experiments for p38α-2P in the presence of ATP. NMR data were processed with TopSpin 2.1 (Bruker) and analyzed with CARA (http://cara.nmr-software.org/downloads/) and Sparky (http://www.cgl.ucsf.edu/home/sparky/).

In the NMR interaction analyses between p38α-2P and the substrate peptides, average CSPs of methyl ^1H-^{13}C correlations are defined as

$$\Delta\omega_{avg} = \sqrt{\Delta\omega_H^2 + \left(\frac{\Delta\omega_C^2}{5.6}\right)}$$

where $\Delta\omega_H$ and $\Delta\omega_C$ are CSPs in ^1H and ^{13}C dimensions, respectively. The scaling factor 5.6 is used in the ^{13}C dimension, which is the ratio of the chemical-shift deviations of methyl ^{13}C and ^1H nuclei deposited in the Biological Magnetic Resonance Data Bank.

© 2014 Nature America, Inc. All rights reserved.

doi:10.1038/nsmb.2861

NMR resonance assignments of p38α. Backbone resonance assignments of p38α were performed with standard TROSY-type triple-resonance NMR spectra, including HNCA, HN(CO)CA, HNCACB, HN(CO)CACB, HNCO and HN(CA)CO. For the assignments of p38α-2P in complex with the ATP analog, alanine, phenylalanine, histidine, methionine, threonine and tyrosine ^{15}N-amino acid–type selectively labeled p38α-2P were also used. The completeness percentage of the assignments for unphosphorylated p38α, p38α-2P and p38α-2P bound to the ATP analog were 61%, 59% and 48% of 342 nonproline residues, respectively. The completeness of the assignment for the unphosphorylated p38α was the same as that reported previously (BMRB 6468)[56]. As discussed above, incomplete assignments are mainly due to the intrinsic local dynamics of p38α.

Assignments of the ILVM-methyl resonances were performed by combining mutational analyses, *J* coupling–based triple-resonance experiments ((H)CC(CO)NH, H(CCCO)NH, and HCCH-TOCSY experiments), and an intermethyl ^{1}H-^{1}H NOE network analysis based on the crystal structures. For the ILVM-methyl resonances, assignments were achieved for 95%, 95% and 78% of all 152 methyl resonances in apo-p38α, apo-p38α-2P and the p38α-2P bound to the ATP analog, respectively. As for the isoleucine-δ1 and methionine-ε resonances, more than 90% of the resonances were assigned under all experimental conditions. These assignments provided highly sensitive site-specific information for all of the functional elements in p38α.

Preparation of the p38α-specific phosphatases PPM1A and HePTP. The cDNA clones encoding human protein phosphatase Mg^{2+}/Mn^{2+} dependent 1A (PPM1A) and hematopoietic protein tyrosine phosphatase (HePTP) were gifts from N. Goshima (AIST), and were originally from the NEDO full-length human cDNA sequencing project. The information about these clones is available in the Human Gene and Protein Database (HGPD) (http://hgpd.lifesciencedb.jp/cgi/)[60,61]. DNA fragments corresponding to amino acid residues 15–339 of PPM1A and 1–382 of HePTP were amplified by PCR. The PPM1A fragment was ligated into the pET28a vector (Merck Millipore) without a purification tag, whereas the HePTP fragment was ligated into the pET15b vector (Merck Millipore) with an N-terminal His_6 tag. Each of these plasmids was transformed into *E. coli* BL21 (DE3) cells, and the bacteria were grown in LB medium. When the cultures reached an OD_{600} of 0.6, the culture medium was supplemented with 1 mM IPTG and was incubated at 30 °C for 8 h. PPM1A was purified by cation-exchange chromatography and SEC. HePTP was purified by nickel-affinity chromatography and SEC. Dephosphorylation of p38α-2P by these phosphatases was performed with 10 μM p38α-2P in the presence of 0.01 molar equivalent of phosphatases. The reaction was performed in 50 mM MOPS, pH 7.0, 100 mM NaCl, 10 mM $MgCl_2$, 0.1 mM EDTA and 2 mM DTT, for 1 h at room temperature, by following a previously published protocol with minor modifications[11].

Competition experiment between the 334D peptide and MK2 for p38α-2P. In this competition assay, p38α-2P in solution was assayed for binding between the N-terminally GB1-fused 334D peptide (GB1-334D peptide) immobilized on IgG beads and a soluble, longer MK2 fragment (aa 47–400). All proteins or peptides were prepared in a buffer consisting of 50 mM Tris-HCl, pH 7.5, 150 mM NaCl, 2 mM DTT and 0.05% (v/v) Tween 20 (TBST buffer). A 50-μL bead volume of IgG Sepharose 6 Fast Flow (GE Healthcare) was suspended in 300 μL of the 5-μM solution of the GB1-334D peptide and incubated with gentle shaking at 4 °C for 1 h. After the beads were washed three times with 300 μL TBST buffer, they were suspended in 300 μL of the 5 μM solution of p38α-2P and incubated at 4 °C for 1 h. The beads were washed five times with 300 μL of the TBST buffer. Then the beads were suspended in 500 μL of the solution of the longer MK2 fragment, at concentrations of 0.3, 0.6 or 1.2 μM in 500 μL of the TBST buffer, and incubated at 4 °C for 1 h. GB1 was used instead of the GB1-334D peptide, as a control. For the eluate from the control experiment, the solution of the longer MK2 fragment was prepared at 5 μM. Supernatants from the bead suspension in the solution of the longer MK2 fragment were analyzed by SDS-PAGE and transferred to a PVDF membrane. Western blotting of p38α-2P was performed, with a 1:1,000 dilution of the anti-p38 mouse monoclonal antibody (Cell Signaling Technology; 9228S) as the first antibody and a 1:10,000 dilution of horseradish peroxidase (HRP)-conjugated anti-mouse IgG (Santa Cruz Biotechnology; sc-2005) as the second antibody. These antibodies have been verified by the manufacturers to recognize human p38α and mouse IgG, respectively, with validation available on the manufacturers' websites. Bound HRP conjugates were detected by chemiluminescence, derived from the oxidization of luminol catalyzed by HRP in the presence of hydrogen peroxide.

Determination of the affinity of p38α-2P for the ATP analog. The ATP analog was added to 40 μM of ILV methyl–labeled p38α-2P at 0.2, 0.4, 0.5, 0.6, 0.7, 0.8, 1.0 and 1.5 mM in the absence of the D peptide, and at 20, 40, 60, 80, 100 and 200 μM concentrations in the presence of a 1.1 equimolar amount of the D peptide (**Supplementary Fig. 7a**). The resonance from the δ1-methyl group of Ile84 in the ATP-binding site exhibited distinct chemical shifts between the ATP analog–unbound and analog-bound forms. The intensities of the resonance derived from the unbound state were fit by assuming 1:1 binding.

Determination of the affinity of p38α-2P for ATP. The affinity of p38α-2P for ATP was determined by the competition experiment with the ATP analog, with the following relationship:

$$K_{\mathrm{d}}^{\mathrm{ATP}} = K_{\mathrm{d}}^{\mathrm{ATP\,analog}} \times \frac{[\mathrm{p38\alpha^{2P}} \times \mathrm{ATP\,analog}]}{[\mathrm{p38\alpha^{2P}} \times \mathrm{ATP}]} \times \frac{[\mathrm{ATP}]^0 - [\mathrm{p38\alpha^{2P}} \times \mathrm{ATP}]}{[\mathrm{ATP\,analog}]^0 - [\mathrm{p38\alpha^{2P}} \times \mathrm{ATP\,analog}]}$$

where $[ATP]^0$ and $[ATP\ analog]^0$ are the total concentration of each compound (2.5 mM). The concentrations of p38α-2P that bound ATP ($[p38\alpha^{2P} \times ATP]$) and the ATP analog ($[p38\alpha^{2P} \times ATP\ analog]$) were estimated from the intensities of the NMR signals that have distinct chemical shifts in the ATP- and ATP analog–bound states (**Supplementary Fig. 7b**). In both the absence and presence of the D peptide, ^{1}H-^{13}C SOFAST-HMQC spectra of 20 μM ILV methyl–labeled p38α-2P were acquired in the presence of the mixture of 2.5 mM ATP and 2.5 mM ATP analog. The spectra in the presence of either 5 mM ATP or 5 mM ATP analog were used as the reference for the intensity of each state. The experiments were conducted at 10 °C to suppress ATP hydrolysis. The loss of ATP during the experiment was negligible.

Determination of the affinity of p38α-2P for the 334 peptide. 50 μM of ILV methyl–labeled p38α-2P was titrated with the 334 peptide (**Supplementary Fig. 7c**). The 334 peptide was added at 25, 50, 75, 100, 200 and 400 μM in both the absence and presence of 1.1 molar equivalent of the D peptide. The CSPs of the δ1-methyl group of Ile259, which is located near the P+1 site, were fit to a 1:1 binding model, and the dissociation constant was determined.

Determination of the kinetic constants for phosphorylation of the 334 peptide by p38α-2P. Phosphorylation of the [U-^{15}N]334 peptide by p38α-2P was confirmed by MALDI-TOF mass spectrometry with an AXIMA spectrometer (Shimadzu) (data not shown) and by the ^{1}H-^{15}N HSQC spectra before and after p38α-2P treatment (**Supplementary Fig. 7d**). Phosphorylation at Thr334 was confirmed with the T334A mutant of the 334 peptide. The time course of the phosphorylation was monitored by successive measurements of ^{1}H-^{15}N SOFAST-HMQC spectra[62] (**Supplementary Fig. 7d**). The intensity of the resonance derived from the pThr334 exhibited characteristic low field shifts in both dimensions[63]. The 334 peptide at concentrations of 100, 200 and 300 μM was phosphorylated by 10 nM of p38α-2P in the absence and presence of 10 μM D peptide. The kinetic constants were determined by the Lineweaver-Burk plot.

Calculation of normalized reaction efficiency. The normalized reaction efficiency (E) was calculated by the population of the functional trimeric p38α-2P–ATP–phosphoacceptor complex, and the catalytic rates were calculated, assuming the K_{d} and k_{cat} values in **Table 1**. Under physiological conditions, in which $[ATP]_{tot} >> [p38]_{tot}$, $[substrate]_{tot}$, E is described by the equation $E = A \times k_{cat} \times ([ATP]_{tot} / K_{\mathrm{d}}^{\mathrm{ATP}} + [ATP]_{tot})$. A is a constant, which includes p38α.

Determination of the affinities of p38α-2P for the docking fragments. The ^{1}H-^{13}C HMQC spectra of ILV methyl–labeled p38α-2P (20 μM) were measured in the presence of increasing amounts of the docking fragment derived from the substrate MEF2A (**Supplementary Fig. 8a**,**b**). The docking fragment was added to p38α at 20, 50, 100, 200, 400 and 500 μM in the absence of the ATP analog, and at 5, 10, 20, 40, 80 and 160 μM in the presence of 4 mM ATP analog (**Supplementary Fig. 8c**,**d**). The CSPs in the δ1-methyl signal of Ile116, which is located in the docking site, were fit to a 1:1 binding model, and the dissociation constant was determined.

© 2014 Nature America, Inc. All rights reserved.

To determine the affinity of p38α-2P for the D peptide, isothermal titration calorimetry (ITC) experiments were performed with a VP-ITC calorimeter (MicroCal) (**Supplementary Fig. 8e**,**f**). The D peptide (500 μM) was added from the syringe to p38α-2P (50 μM) in the isothermal cell by 25 injection steps, in either the absence or presence of 4 mM ATP analog. Experiments were performed at 25 °C. The dissociation constant was determined by fitting the calorimetric data to a 1:1 binding model, with Origin software.

52. Gardner, K.H., Rosen, M.K. & Kay, L.E. Global folds of highly deuterated, methyl-protonated proteins by multidimensional NMR. *Biochemistry* **36**, 1389–1401 (1997).
53. Rosen, M.K. *et al.* Selective methyl group protonation of perdeuterated proteins. *J. Mol. Biol.* **263**, 627–636 (1996).
54. Underwood, K.W. *et al.* Catalytically active MAP KAP kinase 2 structures in complex with staurosporine and ADP reveal differences with the autoinhibited enzyme. *Structure* **11**, 627–636 (2003).
55. Kinoshita, E., Takahashi, M., Takeda, H., Shiro, M. & Koike, T. Recognition of phosphate monoester dianion by an alkoxide-bridged dinuclear zinc(II) complex. *Dalton Trans.* **21**, 1189–1193 (2004).
56. Vogtherr, M. *et al.* NMR backbone assignment of the mitogen-activated protein (MAP) kinase p38. *J. Biomol. NMR* **32**, 175 (2005).
57. Tugarinov, V., Hwang, P.M., Ollerenshaw, J.E. & Kay, L.E. Cross-correlated relaxation enhanced ^{1}H-^{13}C NMR spectroscopy of methyl groups in very high molecular weight proteins and protein complexes. *J. Am. Chem. Soc.* **125**, 10420–10428 (2003).
58. Goto, N.K., Gardner, K.H., Mueller, G.A., Willis, R.C. & Kay, L.E. A robust and cost-effective method for the production of Val, Leu, Ile (δ1) methyl-protonated 15N-, 13C-, 2H-labeled proteins. *J. Biomol. NMR* **13**, 369–374 (1999).
59. Amero, C. *et al.* Fast two-dimensional NMR spectroscopy of high molecular weight protein assemblies. *J. Am. Chem. Soc.* **131**, 3448–3449 (2009).
60. Maruyama, Y. *et al.* Human Gene and Protein Database (HGPD): a novel database presenting a large quantity of experiment-based results in human proteomics. *Nucleic Acids Res.* **37**, D762–D766 (2009).
61. Maruyama, Y. *et al.* HGPD: Human Gene and Protein Database, 2012 update. *Nucleic Acids Res.* **40**, D924–D929 (2012).
62. Schanda, P., Kupce, E. & Brutscher, B. SOFAST-HMQC experiments for recording two-dimensional heteronuclear correlation spectra of proteins within a few seconds. *J. Biomol. NMR* **33**, 199–211 (2005).
63. Selenko, P. *et al. In situ* observation of protein phosphorylation by high-resolution NMR spectroscopy. *Nat. Struct. Mol. Biol.* **15**, 321–329 (2008).

© 2014 Nature America, Inc. All rights reserved.

doi:10.1038/nsmb.2861